

Mott and spin-Peierls physics in TiPO_4 under high pressure

H. Johan M. Jönsson¹, Marcus Ekholm^{1,2}, Silke Biermann^{3,4,5,6}, Maxim Bykov^{7,8}, and Igor A. Abrikosov^{1,9}

¹*Theory and Modelling, IFM-Material Physics, Linköping University, SE-581 83, Linköping, Sweden*

²*Swedish e-Science Research Centre (SeRC), Linköping University, SE-581 83, Linköping, Sweden*

³*CPHT, CNRS, Ecole Polytechnique, Institut Polytechnique de Paris, F-91128 Palaiseau, France*

⁴*Collège de France, 11 place Marcelin Berthelot, 75005 Paris, France*

⁵*Department of Physics, Division of Mathematical Physics,
Lund University, Professorsgatan 1, 22363 Lund, Sweden*

⁶*European Theoretical Spectroscopy Facility, 91128 Palaiseau, France, Europe*

⁷*Laboratory of Crystallography, University of Bayreuth, 95440 Bayreuth, Germany*

⁸*Bayerisches Geoinstitut, University of Bayreuth, 95440 Bayreuth, Germany and*

⁹*Materials Modeling and Development Laboratory,
National University of Science and Technology 'MISIS', Moscow, 119049, Russia*

TiPO_4 is a Mott insulator and one of few inorganic compounds featuring a spin-Peierls phase at low temperature. Recent experimental studies have suggested the presence of spin-Peierls dimerization also at ambient temperature though at high pressure. Here, we present a combined experimental and theoretical study of the energetics of the high-pressure phase. We analyse dimerization properties and their coupling to spin degrees of freedom. Most importantly, we argue that TiPO_4 presents a direct analogue to the celebrated binary transition metal oxide VO_2 . TiPO_4 allows to assess spin-dimer physics in the high-pressure regime in a controlled fashion, having the potential to become an important model system representative of the class of dimerized transition metal oxides.

I. INTRODUCTION

Compounds with strong electronic Coulomb correlations are a hot topic of modern solid state physics. Indeed, electronic correlations may lead to promising phenomena, such as metal-insulator transitions, colossal magnetoresistance¹ or high temperature superconductivity². Moreover, a theoretical description of the underlying interacting many-body system is highly challenging. Incomplete screening of electronic interactions can lead to short-lived quasiparticles and breakdown of Fermi liquid theory. A typical example is the Mott metal-to-insulator transition at low temperature, in which the electron-electron repulsion energy dominates over the kinetic energy, resulting in localisation of the electrons to the atomic sites, and loss of conductivity.

Furthermore, the charge, spin and orbital degrees of freedom may be coupled to the lattice in a non-trivial fashion. This may lead to highly interesting effects, especially in low dimensional materials, such as the spin-Peierls transition. This effect may be observed in systems with (quasi-) one-dimensional spin chains. CuGeO_3 was the first inorganic compound showing this transition, which takes place below 14 K³. More recently, the spin-Peierls effect was observed in the Mott insulator TiOCl at low temperature^{4,5}. Theoretical and experimental studies of TiOCl reveal the strongly correlated nature of this compound and the need to go beyond the static mean-field description of d-d interactions⁶ as well as to include non-local interactions to describe its electronic structure^{7,8}. Remarkably the spin-Peierls effect in TiOCl has been reported at temperatures up to 215 K when subjected to pressure⁹. These results were interpreted as an enhancement of the magnetic interaction energy at high pressure due to increased overlap between the adjacent d

orbitals.

In this work we study the TiPO_4 system, which also has been reported to undergo a spin-Peierls transition, at room temperature, at high pressure¹⁰. We investigate the interplay between the Ti dimerization and electronic structure from ab-initio calculations as well as experiments.

At ambient conditions, TiPO_4 crystallizes in the CrVO_4 structure (space group $Cmcm$), referred to as phase I. Tilted, edge-sharing TiO_6 octahedra form quasi-one-dimensional chains along the c -axis, interconnected by PO_4 tetrahedra (Fig. 1a). Early measurements of magnetic susceptibility¹¹ and neutron diffraction scattering¹² failed to detect magnetic ordering down to 2 K. Subsequent susceptibility measurements combined with nuclear magnetic resonance (NMR)¹³ indicated antiferromagnetic coupling along the chains, with a singlet formation below 74 K: the Ti atoms form dimers within the chains, with alternating Ti-Ti distances, $d \pm \delta$, a phenomenon interpreted as a spin-Peierls transition¹⁴.

When subject to pressure above 4.5 GPa at room temperature, TiPO_4 enters the incommensurately modulated crystallographic phase II. At 7 GPa, the commensurate phase III (space group $P2_1nm$) sets in, which is a four-fold superstructure of phase I, where the Ti-atoms again form dimers. The TiO_6 octahedra are seen to be tilted with respect to the crystallographic b axis. From X-ray diffraction experiments it has been found that among the octahedra chains, there are 4 different tilt angles, ranging from 5° to 9° (for experimental details see supplementary information). In this sense, one may speak of 4 different Ti chains. As can be seen in Fig. 1 chains 1 and 3 lie in the same $[010]$ -plane and are equally dimerized. However, the Ti-Ti distances $d \pm \delta$ are modulated out of phase with respect to each other. This is also true for chains 2

and 4. Reminiscent of phase I, the observed dimerisation has therefore been proposed as an extraordinary case of a spin-Peierls transition occurring at room temperature¹⁰.

In fact, the physics of TiPO_4 is in many respects reminiscent of that of VO_2 , a time-honored and particularly intriguing example of a transition metal oxide. The binary oxide VO_2 displays a first-order metal-insulator transition as a function of temperature, switching from a high-temperature bad metal phase to a low-temperature insulator. While VO_2 was early on invoked as an example of a Mott transition¹⁵, it became clear over the years that the accompanying structural changes – from a high-temperature rutile to a low-temperature monoclinic phase – also played a role in the transition, opening a decade-long debate^{16–18}. Indeed, the structural transition proceeds via a doubling of the unit cell along the crystallographic c -axis and a dimerization and slight tilting of vanadium atoms along chains in that direction. Cluster Dynamical Mean Field Theory calculations^{19,20} characterized the phenomenon as "correlation-assisted Peierls transition", establishing that the insulating phase emerges from the metallic one thanks to (1) a rearrangement of charge within the t_{2g} manifold that leaves the single electron per V atom fully in the a_{1g} orbitals and (2) the formation of a spin singlet ground state in the bonding combination of these a_{1g} states of neighboring vanadium atoms in the dimers. The resulting picture is in agreement with the measured flat magnetic susceptibilities in the insulating phase²¹ and is confirmed by photoemission spectroscopy²².

Investigation of VO_2 remains an active field of research for several reasons: (1) The transition takes place at temperatures of around 340 K, that is, slightly above room temperature, making the compound an ideal material for applications exploiting the metal-insulator transition. In this respect, it is particularly interesting that the transition temperature can be systematically lowered by tungsten substitution²³, although the precise mechanism of this effect is not yet understood. (2) Despite the undoubtable role of the structural distortions in the transition, various variations of the phenomenon indicate the simultaneous presence of strong electronic correlations. Pouget et al. pointed out²¹, that uniaxial stress or tiny amounts of Cr-doping modify the distortions – in particular leaving half of the V atoms undimerized – while still inducing an insulating phase. In the same vein, pump-probe experiments suggest that structural and electronic transitions can be decoupled²⁴. Finally, introducing oxygen vacancies into the system eventually suppresses the transition altogether²⁵. All these elements suggest VO_2 -derived materials or – more generally – materials where dimerization of transition metal ions plays a role are still hiding rich and interesting – and potentially useful – physics. It is therefore intriguing to have, with TiPO_4 , another material at hand sharing various aspects of dimerization physics with VO_2 .

TABLE I: Comparison of calculated equilibrium, equilibrium volume V_0 , bulk modulus B_0 and its pressure derivative B' , parameters and their room temperature experimental values

	V_0 [$\text{\AA}^3/\text{atom}$]	B_0 [GPa]	B'
LDA	10.37	109.92	4.97
LDA+U, U = 2.00 eV	10.78	87.12	5.39
LDA+U, U = 3.00 eV	10.94	89.26	4.90
Experiment ¹⁰	11.16	72	6.5

II. METHODOLOGY

Calculations were performed using density functional theory^{26,27}, with the projector augmented wave (PAW) method²⁸ implementation in the Vienna ab initio simulation package^{29,30} (VASP). For the exchange-correlation functional the local density approximation, with on-site interaction (LDA+U) as parametrized by Dudarev et al.³¹ was used, we chose $U = 2.0$ eV, as will be motivated in section III.

In order to achieve good convergence with regards to the plane wave energy an energy cut-off of 520 eV was chosen. For the Brillouin zone integration we employed a Monkhorst-Pack k-point grid of dimension $5 \times 7 \times 11$, resulting in a total of 112 k-points in the irreducible Brillouin zone. The unit cells used for the calculations, shown in Fig. 1, contained 4 and 8 formulae units respectively.

Details on the experiments are provided in the supplemental materials³².

III. RESULTS AND DISCUSSION

First, we have calculated the total energy as a function of unit cell volume, relaxing the ionic positions at each volume. The equilibrium parameters obtained from our fit to the Birch-Murnaghan equations of state are summarised in Tab. I, also plotted in Fig. 2. As can be seen LDA underestimates the equilibrium volume of the unit cell and slightly overestimates the bulk modulus. Using LDA+U we improve V_0 and B_0 . The pressure dependence of the lattice parameters is plotted in Fig. 3. We find that LDA + U with $U = 2.00$ eV shows best agreement with experiments.

We note that according to our calculations at the theoretical equilibrium volume chains 1 through 4 in figure 1b become equivalent, and the optimized structure therefore becomes equivalent to phase I. At this volume the Ti - O - Ti angle is 94.5° . For comparison, we have carried out calculations at the experimental room temperature volume (see Table I) and have obtained the value 96.5° . This can be compared to the experimental value 95.5° .

At the experimental volume the calculated magnetic moment $0.80\mu_B$ can be compared to the value $0.71\mu_B$

found in reference³³ using PBE. In figure 5 the total density of states (DOS) for different pressures is shown. Using LDA+U we correctly reproduce an insulating state⁷. We see an insulating band gap of ≈ 1 eV formed among the d-states. Note that calculations carried out within LDA only yields a pseudo-gap opened due to AFM order. The states are divided into a low-binding energy Ti-d part and a high-binding energy part, dominated by O-p states. The Ti peak below the Fermi energy contains 1 electron per formula unit, which means that the system is in a d^1 configuration. Figure 6 shows the local Ti-3d density of states projected onto irreducible orbitals, Fig. 1c. Degeneracy of the e_g and t_{2g} states is lifted due to the octahedral symmetry. Moreover, we see that the singly occupied d_{xy} -level is pushed below the d_{yz} and d_{xz} -levels as the octahedra are distorted. Figure 7 shows the charge density of the d_{xy} orbital. At ambient pressure, we find that the chains do not dimerize. This observation does not agree with experimental observations for phase I. The disagreement can be explained by the fact that the increase of elastic energy associated with dimerization is not compensated by the energy gain associated with formation of spin singlets, because the latter is not accurately described with the present exchange-correlation functionals. Here we would like to point out that a similar observation has been reported in Ref.³⁴ for TiOCl. At the same time, the overall pressure dependences of the atomic volume (Fig. 2) and lattice constants (Fig. 3) are correctly captured by our calculations. We therefore proceed with the analysis of the evolution of the electronic and magnetic properties of TiPO_4 upon compression.

In Fig. 4 we show the measured Ti dimerization as a function of pressure, along with computational results. At the pressure where phase III is observed experimentally we find that the chains indeed dimerize, although with a somewhat reduced magnitude, as can be seen in Fig. 4. At the volume $0.94 V_0$, which corresponds to a pressure of 6 GPa, the four chains start developing distinct tilting angles and thus become inequivalent, which is characteristic of the phase III structure. The effect can be seen in Fig. 8. In our calculations the transition from phase I into phase III occurs at around 9 GPa, slightly higher than the experimentally observed transition pressure of 7 GPa.

As pressure is increased further we find that the b and c lattice parameters decrease while the lattice constant a remains nearly constant (Fig. 3). This difference in compressibility along different crystallographic directions is in good agreement with experiment¹⁰. Up to 23 GPa two trends can be noticed: Firstly, the z-axis of the octahedra tend to become aligned with the b axis. Secondly, the chains dimerize further.

However, the pressure dependence of the tilt angles is different in the four different chains. In agreement with experiment, we find chains 2 and 3 to display a larger tilt than chains 1 and 4, Fig. 8. At the same time, the Ti-Ti distances, as well as local magnetic moments of Ti

atoms in chains 2 and 4 are equal to each other, as are those of chains 1 and 3, see Figs. 4 and 9. The former two chains dimerize at a quicker rate with pressure, and have smaller magnetic moments. It thus appears that the dimerization is negatively correlated with the magnitude of the local magnetic moments.

The local Ti DOS depicted in Fig. 6 shows that as pressure is increased and the occupied bands broaden, spin up electrons are transferred to the spin down channel, leading to a gradual quenching of magnetic moments. As shown in Fig. 10 the insulating gap is also gradually reduced, and closes completely at a pressure of 28 GPa. Above this point, the system is metallic in our calculations. As the system is metallized, the magnetic moments of Ti atoms in chains 1 and 3 drop sharply and they become similar to those of chains 2 and 4. At the same time, chains 1 and 3 drastically increase their dimerization and become similar to chains 2 and 4 also in this respect. These effects are also visible in the orientation of the octahedra. Chain 3 is tilted and becomes similar to chain 2, while chain 1 is straightened out to become similar to chain 4, being nearly aligned with the b-direction. In the metallic regime the chains thus have the same interatomic distances and magnetic moments, but the unit cell is characterized by two distinguishable chains with different tilt angles. Both chains are dimerized, but one is more tilted than the other. Increasing pressure further in the metallic regime, we find that the dimerization start to decrease in both chains, although they retain a significant degree of dimerization. The high-pressure phase of TiPO_4 is thus strongly reminiscent of the so-called M_2 phase of VO_2 , which can be induced by uniaxial pressure or minute amounts of Cr-doping.

It appears that the metallization is directly connected with dimerization of the chains. By freezing the internal coordinates of the atoms in the unit cell, and rescaling the lattice constants according to Fig. 3, we find that the bands broaden much slower and that the magnitude of the gap remains the same even up to the highest pressure considered in our calculations (see Fig. 5).

It is important to point out that there is a subtlety concerning the choice of symmetries – non-magnetic or antiferromagnetic – in the calculations. Experimentally, the TiPO_4 phase I has been suggested to form a singlet dimer phase at low temperatures¹³. There is thus no magnetic order. Nevertheless we choose in the calculations to allow for antiferromagnetic ordering. Indeed, we argue that the energetics of a dimerized phase can be expected to be qualitatively and semi-quantitatively well described by a mean-field calculation when (artificially) allowing for antiferromagnetic ordering.

The reason can be seen on the simple example of the Hubbard dimer³⁵. At half filling the ground state of a Hubbard dimer defined by hopping t and Hubbard interaction U is a spin singlet, and its energy reads:

$$E_0 = \frac{U}{2} - \frac{1}{2} \sqrt{U^2 + (4t)^2} \quad (1)$$

At large interaction $U \gg t$, $E_0 = -\frac{4t^2}{U}$ corresponds to the spin fluctuation energy gain. A mean field theory preserving the spin singlet symmetry (unrestricted Hartree-Fock) yields the energy $\frac{U}{2} - 2t$, while an antiferromagnetic mean field solution yields $-\frac{2t^2}{U}$. While the slope of the energy gain with t is thus wrong by a factor of 2, it is clear that the antiferromagnetic solution describes the energetics of the system at least semi-quantitatively, while the paramagnetic solution does not.

The above discussion is a special case of the well-known symmetry dilemma of density functional theory³⁶, stating that – when approximate functionals are used – Kohn-Sham solutions that do not respect the symmetry of the physical ground state but rather introduce artificial symmetry breakings can yield better energetics than Kohn-Sham solutions with the correct symmetry of the physical ground state. For this reason, in our calculations, we allow for antiferromagnetic order of the magnetic moments along the chains in the c -direction of the considered supercells. Of course, further experiments as well as theoretical studies, e.g. cluster DMFT, are highly desirable to clarify the nature of magnetism in phase III.

IV. SUMMARY AND CONCLUSIONS

We have investigated the evolution of the crystal structure of TiPO₄ from ambient to high pressure, considering phases I and III, by means of theoretical calculations employing the LDA+U method. Though at ambient pressure we do not detect any dimerization of the Ti atoms chains, similar to the spin-Peierls compound TiOCl³⁴, as pressure increases, we find that the chains start to dimerize. The four Ti chains react differently to pressure in the insulating phase but become equally dimerized as the system is metallized. Remarkably, the dimerization persists even in the metallic regime, where the magnetic moments of the Ti atoms are very small. Moreover, if the internal coordinates of atoms in the simulation cell are kept fixed to their undimerized positions and the lattice

constants are simply rescaled, we find the metallization to occur at a much higher pressure (smaller volume).

Our results thus indicate that the insulator-to-metal transition is interlinked with the dimerization of the chains at high pressure. The gradual loss of magnetism upon compression observed in our calculations seems to increase the dimerization of the chains. Although our calculations quantitatively underestimate the degree of dimerization, they capture a picture of the influence of pressure on the crystal structure qualitatively correctly. This adds an interesting new aspect to the physics of the quasi-one dimensional Ti chains in TiPO₄, the metallization must be considered as an important part of the process.

We suggest that TiPO₄ represents an interesting new model system for studies of the interplay between the Mott insulator-to-metal transition and the spin-Peierls effect, and that further studies on TiPO₄ should include non-local correlation effects, which are known to be important in both TiOCl and VO₂.

ACKNOWLEDGEMENTS

This project is funded by the Knut and Alice Wallenberg Foundation (Wallenberg Scholar grant No. KAW-2018.0194). We are grateful to the Swedish e-Science Research Centre (SERC) for financial support. I.A.A. gratefully acknowledges the Swedish Research Council (VR) grant No. 2015-04391 and the Swedish Government Strategic Research Area in Materials Science on Functional Materials at Linköping University (Faculty Grant SFO-Mat-LiU No. 2009 00971). The computations were performed on resources provided by the Swedish National Infrastructure for Computing (SNIC) at High Performance Computing Center North (HPC2N) and National Supercomputer Centre (NSC). We further acknowledge support by the European Research Council (Project CorrelMat 617196) and IDRIS GENCI Orsay (project 0901393) at the beginning of the project.

-
- ¹ E. Dagotto, *Science* **309**, 257 (2005), <http://science.sciencemag.org/content/309/5732/257.full.pdf>.
- ² E. A. Stepanov, L. Peters, I. S. Krivenko, A. I. Lichtenstein, M. I. Katsnelson, and A. N. Rubtsov, *npj Quantum Materials* **3**, 54 (2018).
- ³ M. Hase, I. Terasaki, K. Uchinokura, M. Tokunaga, N. Miura, and H. Obara, *Phys. Rev. B* **48**, 9616 (1993).
- ⁴ A. Seidel, C. A. Marianetti, F. C. Chou, G. Ceder, and P. A. Lee, *Phys. Rev. B* **67**, 020405 (2003).
- ⁵ M. Shaz, S. van Smaalen, L. Palatinus, M. Hoinkis, M. Klemm, S. Horn, and R. Claessen, *Phys. Rev. B* **71**, 100405 (2005).
- ⁶ T. Saha-Dasgupta, A. Lichtenstein, and R. Valentí, *Phys. Rev. B* **71**, 153108 (2005).
- ⁷ T. Saha-Dasgupta, A. Lichtenstein, M. Hoinkis, S. Glawion, M. Sing, R. Claessen, and R. Valentí, *New Journal of Physics* **9**, 380 (2007).
- ⁸ M. Aichhorn, T. Saha-Dasgupta, R. Valentí, S. Glawion, M. Sing, and R. Claessen, *Phys. Rev. B* **80**, 115129 (2009).
- ⁹ C. R. Rotundu, J. Wen, W. He, Y. Choi, D. Haskel, and Y. S. Lee, *Phys. Rev. B* **97**, 054415 (2018).
- ¹⁰ M. Bykov *et al.*, *Angewandte Chemie International Edition* **55**, 10.1002/anie.201608530 (2016).
- ¹¹ N. Kinomura, F. Muto, and M. Koizumi, *Journal of Solid State Chemistry* **45**, 252 (1982).
- ¹² R. Glaum, M. Reehuis, N. Stücker, U. Kaiser, and F. Reinauer, *Journal of Solid State Chemistry* **126**, 15 (1996).
- ¹³ J. M. Law, C. Hoch, R. Glaum, I. Heinmaa, R. Stern, J. Kang, C. Lee, M.-H. Whangbo, and R. K. Kremer, *Phys.*

- Rev. B **83**, 180414 (2011).
- ¹⁴ M. Bykov *et al.*, Phys. Rev. B **88**, 10.1103/PhysRevB.88.184420 (2013).
- ¹⁵ N. F. MOTT, Rev. Mod. Phys. **40**, 677 (1968).
- ¹⁶ J. B. Goodenough, Journal of Solid State Chemistry **3**, 490 (1971).
- ¹⁷ R. Eguchi, M. Taguchi, M. Matsunami, K. Horiba, K. Yamamoto, Y. Ishida, A. Chainani, Y. Takata, M. Yabashi, D. Miwa, Y. Nishino, K. Tamasaku, T. Ishikawa, Y. Senba, H. Ohashi, Y. Muraoka, Z. Hiroi, and S. Shin, Phys. Rev. B **78**, 075115 (2008).
- ¹⁸ V. Eyert, Annalen der Physik **11**, 650 (2002).
- ¹⁹ S. Biermann, A. Poteryaev, A. I. Lichtenstein, and A. Georges, Phys. Rev. Lett. **94**, 026404 (2005).
- ²⁰ J. M. Tomczak, F. Aryasetiawan, and S. Biermann, Phys. Rev. B **78**, 115103 (2008).
- ²¹ POUGET, J. P. and LAUNOIS, H., J. Phys. Colloques **37**, C4 (1976).
- ²² T. C. Koethe, Z. Hu, M. W. Haverkort, C. Schüßler-Langeheine, F. Venturini, N. B. Brookes, O. Tjernberg, W. Reichelt, H. H. Hsieh, H.-J. Lin, C. T. Chen, and L. H. Tjeng, Phys. Rev. Lett. **97**, 116402 (2006).
- ²³ X. Tan, T. Yao, R. Long, Z. Sun, Y. Feng, H. Cheng, X. Yuan, W. Zhang, Q. Liu, C. Wu, Y. Xie, and S. Wei, Scientific reports **2**, 466 (2012).
- ²⁴ M. F. Jager, C. Ott, P. M. Kraus, C. J. Kaplan, W. Pouse, R. E. Marvel, R. F. Haglund, D. M. Neumark, and S. R. Leone, Proceedings of the National Academy of Sciences **114**, 9558 (2017), <https://www.pnas.org/content/114/36/9558.full.pdf>.
- ²⁵ L. Fan, X. Wang, F. Wang, Q. Zhang, L. Zhu, Q. Meng, B. Wang, Z. Zhang, and C. Zou, RSC Adv. **8**, 19151 (2018).
- ²⁶ P. Hohenberg and W. Kohn, Phys. Rev. **136**, B864 (1964).
- ²⁷ W. Kohn and L. J. Sham, Phys. Rev. **140**, A1133 (1965).
- ²⁸ P. E. Blöchl, Phys. Rev. B **50**, 10.1103/PhysRevB.50.17953 (1994).
- ²⁹ G. Kresse and J. Furthmüller, Phys. Rev. B **54**, 10.1103/PhysRevB.54.11169 (1996).
- ³⁰ G. Kresse and J. Furthmüller, Computational Materials Science **6**, [https://doi.org/10.1016/0927-0256\(96\)00008-0](https://doi.org/10.1016/0927-0256(96)00008-0) (1996).
- ³¹ S. L. Dudarev *et al.*, Phys. Rev. B **57**, 10.1103/PhysRevB.57.1505 (1998).
- ³² See supplemental materials for details on the experimental methods.
- ³³ S. López-Moreno and D. Errandonea, Phys. Rev. B **86**, 104112 (2012).
- ³⁴ L. Pisani, R. Valentí, B. Montanari, and N. M. Harrison, Phys. Rev. B **76**, 235126 (2007).
- ³⁵ J. M. Tomczak, *Spectral and Optical Properties of Correlated Materials.*, Theses, Ecole Polytechnique X (2007).
- ³⁶ J. P. Perdew, A. Savin, and K. Burke, Phys. Rev. A **51**, 4531 (1995).

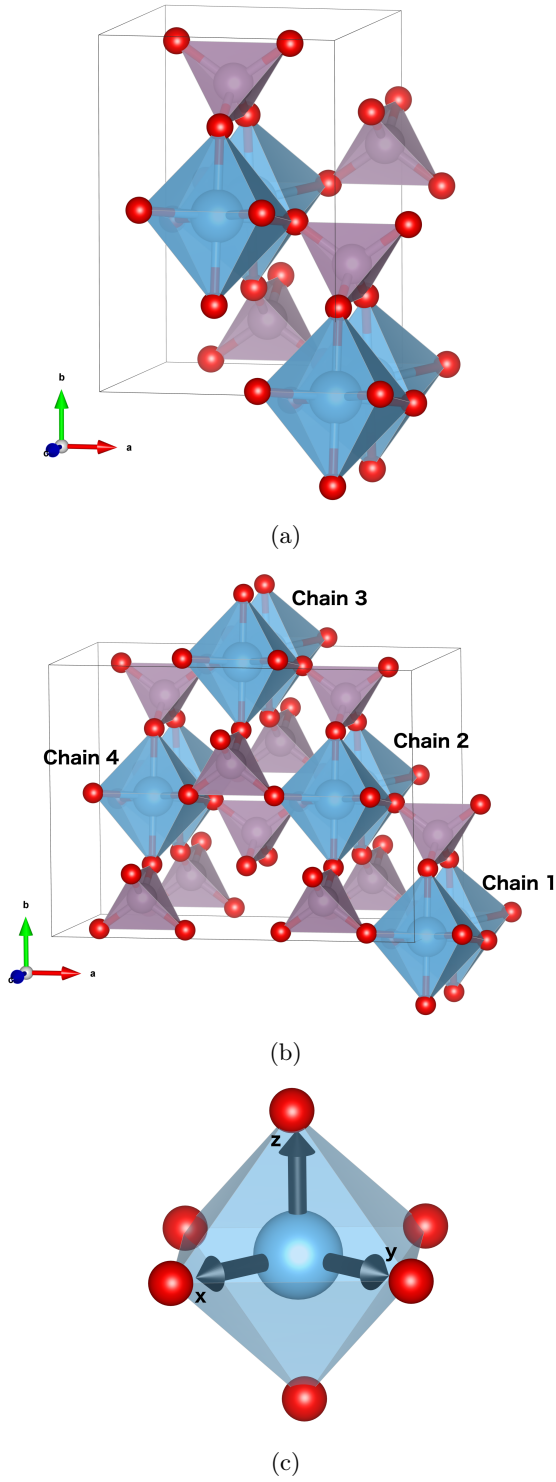


FIG. 1: Crystal structure of a) phase I (space group $Cmc21$) and b) phase III (space group $P2_1nm$) of TiPO_4 . Ti atoms are shown in blue, P are purple and O are red. Also shown in blue are the Ti-O complexes and the P-O complexes are purple. Panel c) shows a schematic picture of the local coordinate system (defined as x, y, z) around a given Ti atom used for the calculation of projected density of states. The Ti chains lie along the $x + y$ line.

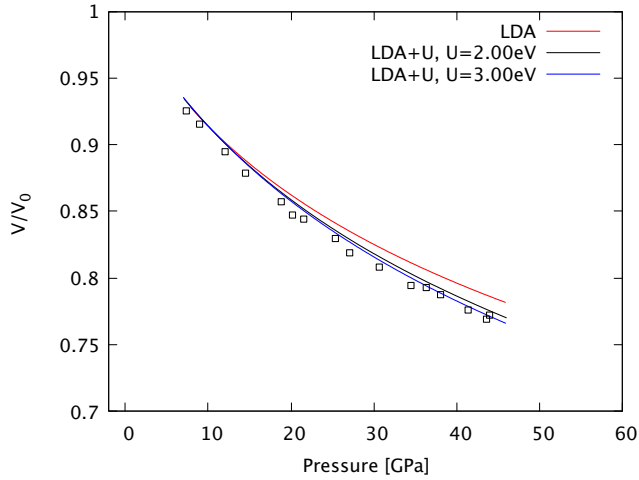


FIG. 2: Equations of state calculated using LDA, LDA+U with $U=2.00$ eV and LDA+U with $U=3.00$ eV. Experimental results¹⁰ are marked with open squares. Volume per atom, V , is shown relative to the equilibrium volume V_0 . Calculations use the calculated zero pressure volume for V_0 and experiments the experimentally obtained zero pressure volume.

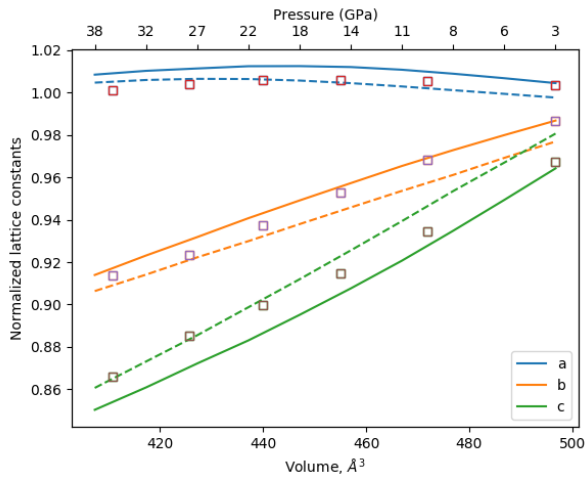


FIG. 3: Calculated pressure dependence of the lattice constant a , b , and c normalized by their calculated values at zero pressure. Solid lines show values obtained using LDA + U with $U=2.0$ eV, dashed lines show values obtained with $U=3.0$ eV. Open symbols are experimental values¹⁰.

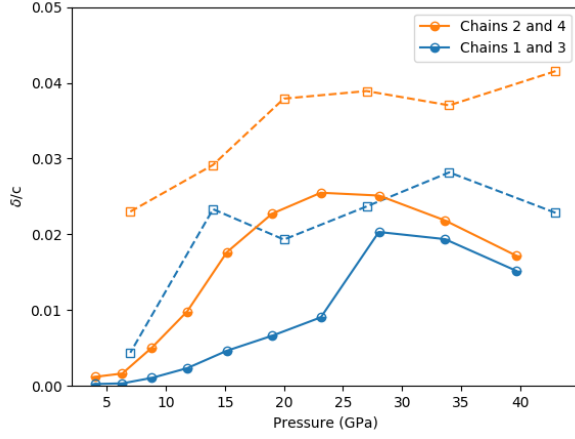


FIG. 4: Dimerization along the c -axis, $\delta = d_{T_i-T_i} - c/2$, of chains 1 to 4 normalized by the c -lattice parameter. See Fig. 1 for the details of the crystal structure and designation of the chains. Experimental values are shown as open squares connected by dashed lines, calculated values are denoted by filled circles, for experimental details please see supplementary information³².

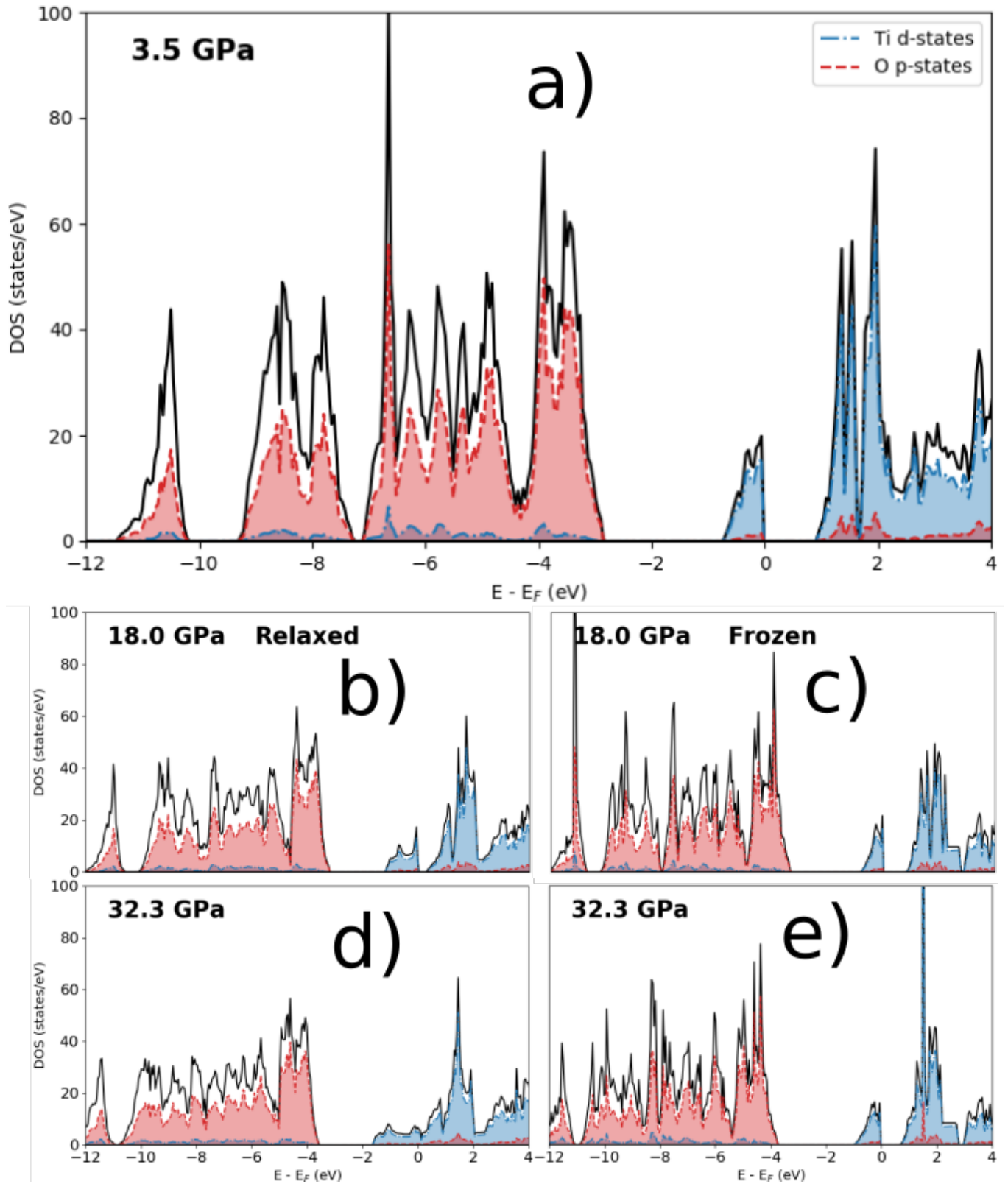
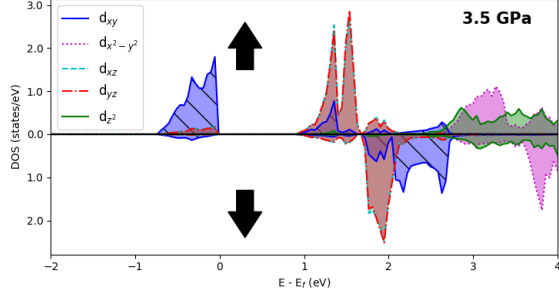
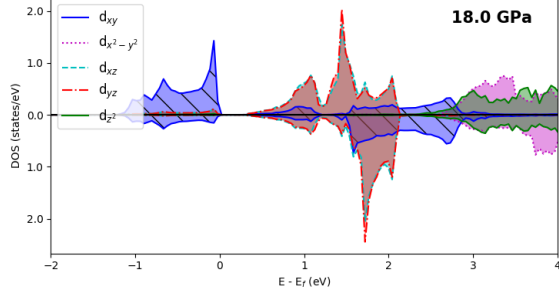


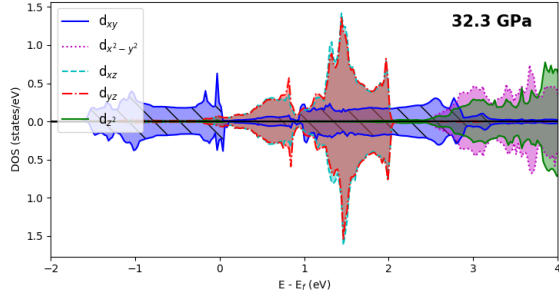
FIG. 5: Total electronic density of states as a function of energy E , relative to the Fermi energy E_F , calculated at three different pressures, (a) 3.5 GPa, (b, c) 18.0 GPa and (d, e) 32.3 GPa. Panels (b) and (d) show results of fully relaxed calculations. Panels (c) and (e) show the results of calculations with ionic positions fixed to those obtained for the relaxed structure at 3.5 GPa.



(a)

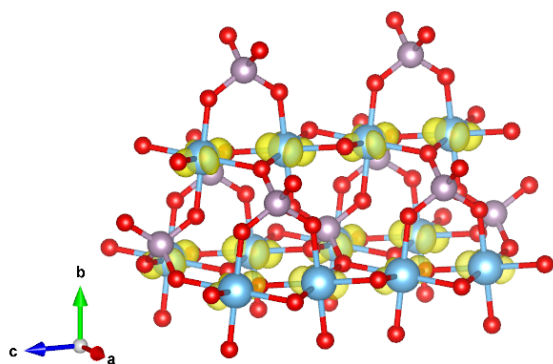


(b)

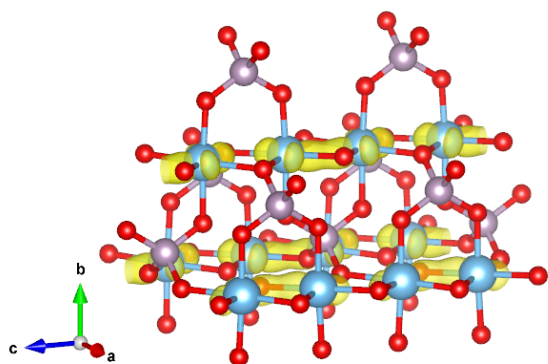


(c)

FIG. 6: Spin polarized electronic density of states projected onto the d-orbitals centered at a given Ti atom in the unit cell, as a function of energy E relative to the Fermi energy E_F , calculated at three different pressures, (a) 3.5 GPa, (b) 18.0 GPa and (c) 32.3 GPa. The spin up channel is depicted on the upper half of the y-axis and the spin down channel on the lower half.



(a)



(b)

FIG. 7: Partial charge density of the d_{xy} -orbital calculated at pressures of (a) 3.5 and (b) 32 GPa.

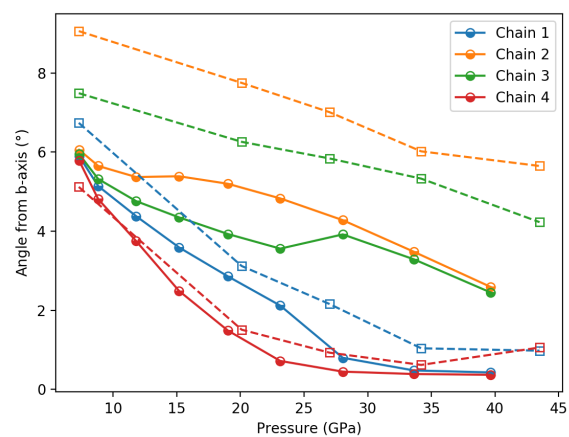


FIG. 8: Angle between b-axis and octahedral major axis as a function of pressure for the four different Ti-chains. See Fig. 1 for the details of the crystal structure and designation of the chains. Experimental values (see supplementary information³²) are shown with open squares connected by dashed lines, half filled circles denote calculated values.

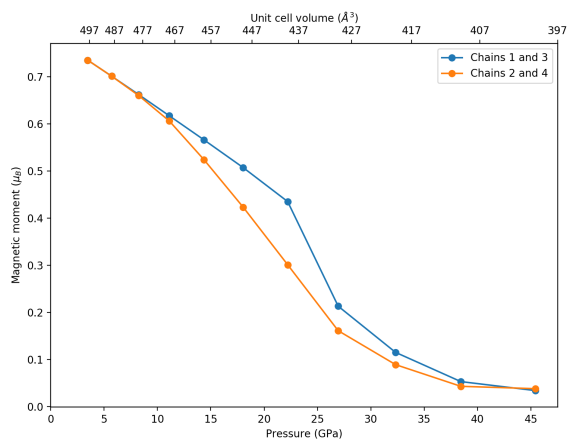


FIG. 9: Calculated magnetic moments of Ti atoms, obtained in simulations of phase III with induced AFM order using the LDA+U method, as a function of pressure. Unit cell volume is shown on the upper x-axis.

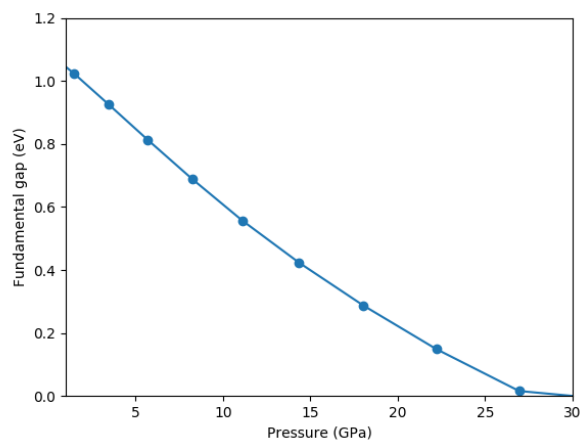


FIG. 10: Calculated fundamental gap as a function of pressure.